Gyro-kinetic analyses of impurity transport within varying triangularity, high-density spherical tokamak plasmas with GENE

A. Bhattacharya [1]

[1] *Independent Researcher, Kolkata 700119, West Bengal, India*

Abstract

The study here shows the effects of shape optimization parameters such as plasma triangularity (δ) on anomalous transport of impurity species within high density L-mode spherical tokamak plasmas. Impurities are non-fuel species within plasma that can hinder the confinement by means of radiation losses or fuel dilution and therefore prevent a long-pulse sustenance. The impurity element analyzed here is the low Z carbon (C, Z = 6). Theoretical design of a spherical tokamak (ST) configuration is used for simulating varying triangularity steady-state plasma conditions within them using the open-source Grad-Shafranov equation solver FreeGS. While the theoretical ST design shown here does not belong to any current operational systems, the design parameters and the parameters characterizing the plasmas simulated within them are in accordance with the existing ST systems worldwide. Shape optimization parameters influence the kinetic (parameter) profile distributions within plasmas which in turn influence the type of microinstability that may dominate at a given region of a plasma. Effects from impurity transport on such microinstabilities in varying triangularity, high-density plasmas are analysed in this study using the gyro-kinetic code GENE. Analyses shown here based on GENE results of the FreeGS simulated plasmas provide with insights regarding first, the effects of change in δ on impurity distribution(s) within a plasma and second, whether such change in impurity distribution(s) influence the nature of local microturbulences.

I. Introduction

Impurities are non-fuel species that may sometimes remain unnecessarily present within a plasma (e.g. Oxygen, Carbon, Molybdenum, Tungsten). They undergo collisions with electrons and main ions within the plasma leading to atomic processes such as ionization, recombination and charge-exchange. This is followed by either radiation losses due to transition of the newly formed ions from metastable to ground state or else fuel dilution thereby raising the effective charge state (Z_{eff}) within the plasma [1]. Low Z impurities such as Lithium and Boron are sometimes purposefully injected into plasma in a controlled manner to prevent extensive heating of the divertor region or for suppressing instabilities e.g., type-I ELMs in H-mode plasmas [2]. Thus, impurities can be advantageous or not based on the manner and the reason they get introduced into a plasma and a study of their distributions within the plasma is necessary. Presence of microinstabilities within a plasma effect the transport mechanism at a given region. Such instabilities are triggered based on various local factors such as magnetic field-line curvature, trapped particle fraction, inverse aspect ratio, density and temperature gradients, respectively [3]. The unstable modes can either be dissipative or reactive in nature which is assessed using gyrokinetic codes [4]. Plasma triangularity (δ) and squareness (ζ) quantify the arrangement of field lines at the separatrix (and within plasma) thus describing the plasma shape. Difference in these quantities within separate steady-state plasma equilibria differ their kinetic pressure p(ψ), poloidal current density function f(ψ) and their gradient (p', ff') distributions, respectively. This then vary the local conditions responsible for the onsets of microinstabilities at a radial location. This study attempts to understand the effects of δ and ζ on triggering (or suppressing) microinstabilities by analyzing the same radial location in the outboard (low-field) region of two separate plasma equilibria. A particular

emphasis is on change in impurity ion distributions due to plasma shape change and the influence of such change in determining the nature of unstable modes in the region.

II. Theory and Procedure

Two separate plasma equilibria (PLASMA 1: $R_0 = 0.862$ m, a = 0.504 m, $B_{t,0} = 1.487$ T, $I_p = 1.005$ MA, $\beta_p = 0.400$, $\beta_t = 0.023$, A = 1.709, $\kappa = 2.082$, $\delta = 0.292$, $\zeta_{out} = -0.185$, X-point coordinates = [(0.715 m, 1.05 m), (0.715 m, −1.05 m)], $q_0 = 0.493$, $q_a = 3.461$, $f_{GW} = 1.25$ and PLASMA 2: R_0 = 0.795 m, a = 0.492 m, $B_{t,0} = 1.487$ T, $I_p = 0.627$ MA, β_p = 0.127, $\beta_t = 0.002$, A = 1.616, $\kappa = 2.136$, $\delta = 0.158$, ζ_{out} = −0.224, X-point coordinates = [(0.717 m, 1.05 m), (0.717 m, −1.05 m)], $q_0 = 1.013$, $q_a = 5.523$) are modelled within an arbitrary spherical tokamak (ST) design using the Grad Shafranov equation solver FreeGS [5] as shown in fig. (1). It is noted here that the rough wall design and poloidal field (PF) coil positions in fig. (1) are arbitrary and do not belong to any tokamaks currently built. The parameters poloidal beta (β_p) and net plasma current (I_p) are provided to FreeGS as kinetic constraints for generating the poloidal flux function (ψ (R, Z)) contours and determining the parameters characterizing the plasma conditions shown in fig. (1). Low beta (β) within PLASMA 2, with same toroidal field (B_t) as PLASMA 1, leads to a drop in p(ψ) within PLASMA 2 as seen in fig. (2). With same $T_{e,0} = 1.0$ keV and $T_{i,0} = 4.0$ keV assumed for both plasmas, $n_{e,0}$ (= p_0 / ($T_{e,0}$+$T_{i,0}$)) then drops within PLASMA 2 ($n_{e,0}$ = 2.713E+19 m^{-3}) when compared to PLASMA 1 ($n_{e,0}$ = 2.502E+20 m^{-3}). This drops $n_{e,a}$ as well within PLASMA 2 ($n_{e,a}$ = 5.427E+18 m^{-3}) over PLASMA 1 ($n_{e,a}$ = 4.234E+19 m^{-3}) as $n_{e,a}$ is determined from $n_{e,a} = n_{e,0} (p_a/ p_0)^{1/3}$ [6] where, p_0 and p_a are the central and edge kinetic pressures. With $T_{e,a} \approx T_{i,a}$ assumed, the edge temperature is determined as $T_{e,a} = T_{i,a} = p_a /(2\ n_{e,a})$. Edge temperatures are obtained as $T_{e,a} = T_{i,a} = 0.0716$ keV for PLASMA 1 and 0.100 keV for PLASMA 2. The n_e and T_e waveforms are generated with peaking factors $k_{ne} = 1.75$ and $k_{Te} = 2.05$. The T_i waveforms are generated with $T_i = (p(\psi)/n_e) - T_e$. The n_e, T_e, T_i waveforms for both plasmas are shown in fig. (3a) – (3b). A pure plasma shall follow the density condition $n_e = n_i$ whereas a plasma with impurity shall follow the condition $n_e = n_i + \Sigma\ Z\ n_z$ where, Z – charge state of impurity ion. With enough impurity concentration, the n_e waveform (and hence the density gradient) may change thus

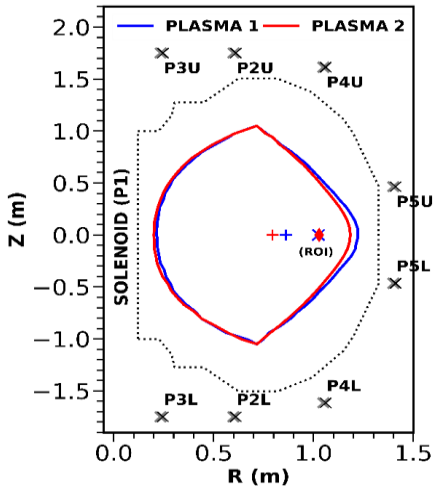

Fig. 1: Magnetic axis (+) and separatrices of PLASMA 1 (blue), PLASMA 2 (red) within rough wall design (black dotted) of an arbitrary ST with PF coil positions (black-x) shown; ROI: Region-Of-Interest (radial) analysed with GENE within the plasmas

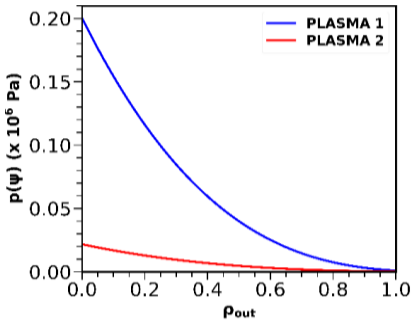

Fig. 2: Kinetic pressure (p(ψ)) within analysed plasmas with respect to their normalized outboard radius (ρ_{out} = r/a)

Notations: R_0 – Major radius (magnetic axis), $B_{t,0}$ – Central toroidal field, a – Minor radius, β_t – Toroidal beta, A – Aspect ratio, κ – Elongation, δ – Triangularity, ζ_{out} – Outboard/Low-field side squareness (upper quadrant), q_0 – Central safety factor, q_a – Edge safety factor, $T_{e,0}$ and $T_{i,0}$ – Central electron and ion temperatures, $n_{e,0}$ and $n_{e,a}$ – Central and edge electron densities, $T_{e,a}$ and $T_{i,a}$ – Edge electron and ion temperatures, n_i, n_z – Main and impurity (charge state Z) ion densities

changing the nature of microinstability dominant at a given region within a plasma. Assessment of impurity ion radial distributions is hence necessary and the impurity species analysed here is Carbon (C). An indigenous impurity transport code (IMPRK4) has been developed for assessing carbon charge state distributions within the two plasmas. The code is written in Python and uses an explicit 4th order Runge-Kutta [7] method in time for solving the radial impurity transport equation (RITE) [8]. The radial derivatives are discretized using a central difference scheme. Similar neutral impurity density $n_{z,0}$ (fig. 3c) and same impurity diffusivity (D_z) and convective velocity (v_z) (fig. 3d) waveforms are provided to IMPRK4 for assessing the carbon ion distributions (fig. 3e – 3f) along the outboard radii of the two plasmas. IMPRK4 uses the effective ionization, recombination and charge-exchange rate coefficients of carbon charge states from the ADAS database [9] for solving the RITE. Carbon ion distributions from IMPRK4 are used to obtain the effective charge state ($Z_{eff} = (n_i + \Sigma\, Z^2\, n_z)/n_e$ with Z = 1 for deuteron as main ions; m_{ref} = 2.014 amu for GENE EV runs) of the two plasmas (fig. 4a).

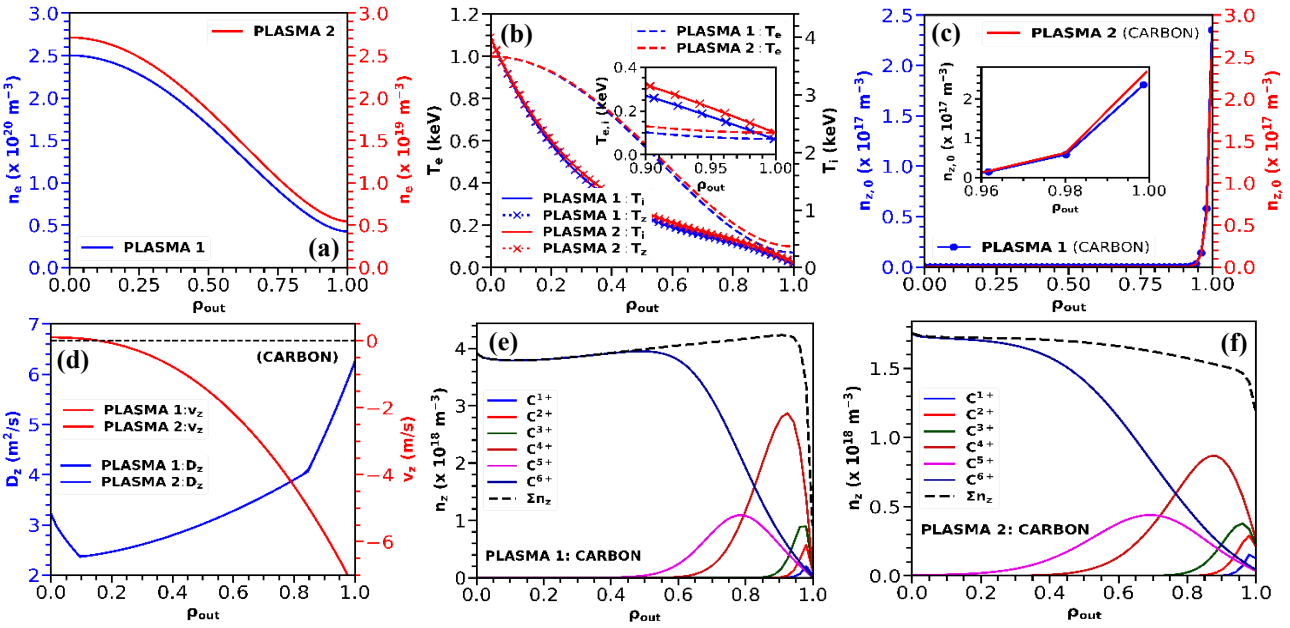

Fig. 3: (a) n_e (m^{-3}), (b) T_e (left: dashed), T_i , T_z (right, solid, dotted-x) (keV), (c) $n_{z,0}$ (m^{-3}), (d) D_z (m^2/s) (left: blue) and v_z (m/s) (right: red) waveforms with respect to ρ_{out} of their plasmas (negative v_z represents inward convection); Radial distributions of carbon ions obtained from IMPRK4 with respect to ρ_{out} within (e) PLASMA 1, (f) PLASMA 2

III. GENE results and Discussions

Line-averaged net impurity densities obtained from the Σn_z (black-dashed) waveforms (sum of all carbon charge state distributions) in fig. (3e) – (3f) yield a carbon concentration of about 4.92% within PLASMA 1 and about 19.68% within PLASMA 2, respectively. A point at the mid-plasma radius (fig. 1) is chosen now as the Region-Of-Interest (ROI) within both plasmas for GENE analyses [10] to understand impurity effects on local microturbulences. Previous work considering the impurity species carbon includes analyses of the transition of microturbulences from ion-branch to multiscale-branch (multiscale turbulence) at the pedestal region of DII-D discharge #164988 (r/a = 0.92) [11]. The study

Notations: R_0 – Major radius (magnetic axis), $B_{t,0}$ – Central toroidal field, a – Minor radius, β_t – Toroidal beta, A – Aspect ratio, κ – Elongation, δ – Triangularity, ζ_{out} – Outboard/Low-field side squareness (upper quadrant), q_0 – Central safety factor, q_a – Edge safety factor, $T_{e,0}$ and $T_{i,0}$ – Central electron and ion temperatures, $n_{e,0}$ and $n_{e,a}$ – Central and edge electron densities, $T_{e,a}$ and $T_{i,a}$ – Edge electron and ion temperatures, n_i, n_z – Main and impurity (charge state Z) ion densities

here also witnesses such multiscale turbulences when considering $Z_{eff} = 1$ (pure plasma) at the ROI of PLASMA 2 (fig. 1). This study however, introduces the impurity effects into GENE Eigen value (EV) computations through mentioning the local Z_{eff} in the 'parameters' file. GENE settings geometry = 'circular' and reference values $L_{ref} = R_0$, $n_{ref} = n_{e,0}$, $B_{ref} = B_{t,0}$, $T_{ref} = T_{e,0}$, respectively, remain same for both plasmas. Further ROI (R = 1.025 m, Z = 0) data for PLASMA 1 are local shear S = 0.805, $\alpha = 0.943$, $Z_{eff} = 1.711$, $r/R_0 = 0.189$, $L_{ref}/L_n = 2.656$, $L_{ref}/L_{Te} = 3.578$, $L_{ref}/L_{Ti} = 6.329$, $n_e/n_{ref} = 0.793$, $T_e/T_{ref} = 0.735$, $T_i/T_{ref} = 1.221$, respectively. Similar ROI (R = 1.028 m, Z = 0) data for PLASMA 2 are S = 1.053, $\alpha = 0.435$, $Z_{eff} = 4.223$, $r/R_0 = 0.294$, $L_{ref}/L_n = 3.430$, $L_{ref}/L_{Te} = 4.796$, $L_{ref}/L_{Ti} = 4.502$, $n_e/n_{ref} = 0.639$, $T_e/T_{ref} = 0.546$, $T_i/T_{ref} = 0.896$, respectively. With these details and with η_i ($= L_n/L_{Ti} = 2.383$) greater than η_e ($= L_n/L_{Te}$) within PLASMA 1, stabilized modes (growth rate $\gamma < 0$ with positive ω) are obtained along ion branch between $0.91 \leq k_y \rho_i \leq 1.0$ for PLASMA 1. No solutions are generated by the EV solver beyond this range. This points to transport phenomenon possibly being neoclassical at the PLASMA 1 ROI. Figures (5a) – (5b) show γ and mode frequency (ω) waveforms at the PLASMA 2 ROI when the local Z_{eff} is set ~ 4.2 (blue) and 1.0 (red) for GENE EV runs. The presence of both, (collisional) Trapped Electron Modes (TEMs) between $1.5 \leq k_y \rho_i \leq 3.0$ and the Electron temperature gradient (ETG) modes once $k_y \rho_i > 3.0$, are realized at the PLASMA 2 ROI when Z_{eff}=1.0. However, with Z_{eff} ~ 4.2 only ETG modes are observed at the PLASMA 2 ROI ($\eta_e = 1.398$) [12]. The observation at higher Z_{eff} is due to impurity (carbon) ions colliding with trapped electrons and turning them into passing electrons thus suppressing the TEMs. Maximum $\gamma \sim 8.4$ obtained for the ETG modes at $k_y \rho_i \sim 29.0$ in both Z_{eff} cases (fig. 5a). Thus, a drop in δ, ζ_{out} in PLASMA 2 over PLASMA 1 lead to – (i) ROI with neoclassical transport witnessing microturbulences, (ii) rising line-averaged n_z/n_e within PLASMA 2. A Z_{eff} (=1.0) drop transitions the local instability from pure η_e to multiscale-branch within PLASMA 2.

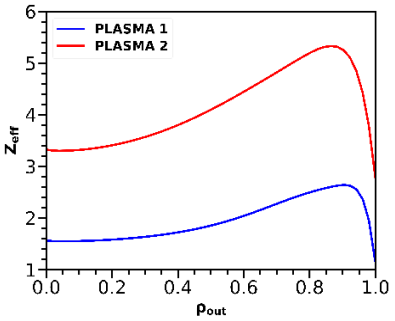

Fig. 4: Z_{eff} (evaluated with single impurity species: carbon) at different regions of the analysed plasmas

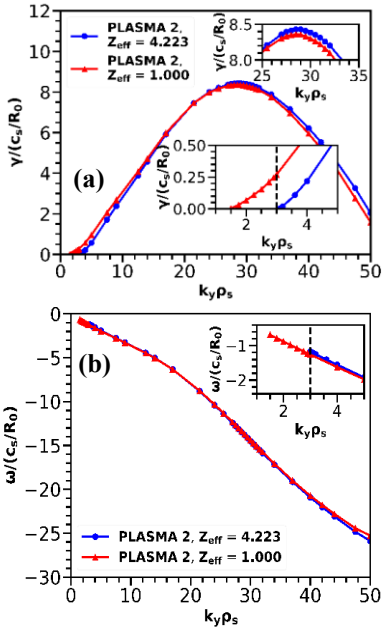

Fig. 4: (a) growth rate γ, (b) mode frequency ω, with respect to $k_y\rho_i$ at [R, Z] = [1.028 m, 0] within PLASMA 2 with Z_{eff} set to 4.233 (blue) and 1.0 (red) for GENE EV runs

References

[1] K. Behringer, 'Description of impurity transport code STRAHL', Report–JET-R(87)08, JET Joint Undertaking (1987)
[2] F. Bagnato, B. P. Duval, O. Sauter, S. Coda, A. Karpushov et al., *Plasma Phys. Control. Fusion* **66** 075019 (2024)
[3] J. Wesson, *Tokamaks*, 4th edition, Oxford University Press Inc., New York (2011)
[4] T. Görler, X. Lapillonne, S. Brunner, T. Dannert, F. Jenko et al., *Journal of Computational Physics* **230** 7053 – 7071 (2011)
[5] https://freegs.readthedocs.io/en/latest/generated/freegs.html, FreeGS manual (as on 06/26/2026)
[6] R. H. Fowler, J. A. Holmes, J. A. Rome, 'NFREYA – A Monte Carlo beam deposition code for noncircular tokamak plasmas', Report – ORNL/TM-6845 (1979)
[7] P. Moin, *Fundamentals of Engineering Numerical Analysis*, Cambridge University Press, 2nd edition, Cambridge (2010)
[8] A. Bhattacharya, J. Ghosh, M. B. Chowdhuri, P. Munshi, I. Murakami et al., *Plasma and Fusion Research* **14** 1403155 (2019)
[9] https://open.adas.ac.uk/documentation, OPEN-ADAS (as on 06/26/2026)
[10] F. Jenko, W. Dorland, M. Kotschenreuther, B. N. Rogers, *Phys. Plasmas* **7(5)** 1904 – 1910 (2000)
[11] E. A. Belli, J. Candy, I. Sfiligoi, *Plasma Phys. Control. Fusion* **65** 024001 (2023)
[12] S.S. Henderson, L. Garzotti, F. J. Casson, D. Dickinson, M. F. J. Fox et al., *Nucl. Fusion* **54** 093013 (2014)

Notations: R_0 – Major radius (magnetic axis), $B_{t,0}$ – Central toroidal field, a – Minor radius, β_t – Toroidal beta, A – Aspect ratio, κ – Elongation, δ – Triangularity, ζ_{out} – Outboard/Low-field side squareness (upper quadrant), q_0 – Central safety factor, q_a – Edge safety factor, $T_{e,0}$ and $T_{i,0}$ – Central electron and ion temperatures, $n_{e,0}$ and $n_{e,a}$ – Central and edge electron densities, $T_{e,a}$ and $T_{i,a}$ – Edge electron and ion temperatures, n_i, n_z – Main and impurity (charge state Z) ion densities